Journal of Power Sources 196 (2011) 6473–6477

Contents lists available at ScienceDirect

Journal of Power Sources

journal homepage: www.elsevier.com/locate/jpowsour

Short communication

Reduced graphene oxide/tin oxide composite as an enhanced anode material for lithium ion batteries prepared by homogenous coprecipitation

Xianjun Zhu[a,b], Yanwu Zhu[b], Shanthi Murali[b], Meryl D. Stoller[b], Rodney S. Ruoff[b,*]

[a] College of Chemistry, Central China Normal University, 152 Luoyu Rd, Wuhan, Hubei 430079, China
[b] Department of Mechanical Engineering and the Texas Materials Institute, The University of Texas at Austin, One University Station C2200, Austin, TX 78712, USA

ARTICLE INFO

Article history:
Received 1 April 2011
Received in revised form 5 April 2011
Accepted 6 April 2011
Available online 12 April 2011

Keywords:
Reduced graphene oxide
Tin oxide
Homogeneous coprecipitation
Lithium ion battery
Anode

ABSTRACT

Reduced graphene oxide/tin oxide composite is prepared by homogenous coprecipitation. Characterizations show that tin oxide particles are anchored uniformly on the surface of reduced graphene oxide platelets. As an anode material for Li ion batteries, it has 2140 mAh g^{-1} and 1080 mAh g^{-1} capacities for the first discharge and charge, respectively, which is more than the theoretical capacity of tin oxide, and has good capacity retention with a capacity of 649 mAh g^{-1} after 30 cycles. The simple synthesis method can be readily adapted to prepare other composites containing reduced graphene oxide as a conducting additive that, in addition to supporting metal oxide nanoparticles, can also provide additional Li binding sites to, perhaps, further enhance capacity.

1. Introduction

Lithium ion batteries are the favored power sources for portable electronic devices such as laptop computers, cellular phones, camcorders, and mp3 players. Graphite is a standard anode material in Li-ion batteries as lithium can insert and deinsert during discharging and charging, respectively, with a theoretical specific capacity of 372 mAh g^{-1} [1]. However, in order to meet the increasing demand for batteries with higher energy densities, it is essential to develop electrodes made from durable, nontoxic, and inexpensive materials with a high charge/discharge rate and a higher reversible capacity. Tin and tin oxides, which have higher theoretical capacities (Sn: 994 mAh g^{-1}, and SnO_2: 782 mAh g^{-1}) compared to graphite, have been proposed as alternative anode materials [2–4]. However, the practical application of tin oxide as an anode is hampered by its poor cyclability, resulting from large volume changes of over 300% during discharge/charge, leading to electrical disconnection from the current collector [5–7]. One approach to circumvent this limitation is to hybridize SnO_2 with carbonaceous materials to better accommodate the strain during volume change [8,9]. On the other hand, graphene has excellent electronic conductivity, high theoretical surface area of 2630 m^2 g^{-1}, good mechanical properties, and can be used as a conducting additive for hybrid nanostructured materials [10–14]. Recently, high surface area chemically modified graphene has been used to form hybrid materials with SnO_2, TiO_2 and Mn_3O_4 nanoparticles with the aim of improving the capacity and cycling stability of the resulting electrode materials [15–17]; it is a challenge to find a good method to prepare reduced graphene oxide (RG-O) and metal oxide composite, resulting in the homogeneous dispersion of metal oxide nanoparticles on the 'graphene' matrix.

We report here a simple method for obtaining RG-O–SnO_2 composite by (i) homogeneous precipitation of $SnCl_4$ in a suspension of graphene oxide (G-O) platelets using urea and (ii) subsequent reduction of the G-O with hydrazine under microwave irradiation to yield RG-O platelets decorated with SnO_2 nanoparticles, and finally (iii) annealing at 500 °C for 3 h under a nitrogen atmosphere with the aim of increasing crystallinity of the SnO_2 nanoparticles. As an anode material for Li-ion batteries, the RG-O/SnO_2 composite exhibited unprecedentedly high discharge and charge capacities of 2140 and 1080 mAh g^{-1}, respectively, for the first cycle, normalized to the mass of SnO_2 in the composite (~1712 and 864 mAh g^{-1} respectively, based on the total mass of the composite), and good cycling performance with 649 mAh g^{-1} capacity at the 30th discharge. Our method of synthesis presents a promising route for large scale production of RG-O platelet/metal oxide nanoparticle composites as electrode materials for Li ion batteries.

2. Experimental

2.1. Synthesis of graphite oxide

Graphite oxide was synthesized from natural graphite by a modified Hummers method. Briefly, graphite powders (2 g; SP-1, Bay

* Corresponding author. Tel.: +1 512 471 4691; fax: +1 512 471 7681.
E-mail address: r.ruoff@mail.utexas.edu (R.S. Ruoff).

0378-7753/$ – see front matter © 2011 Elsevier B.V. All rights reserved.
doi:10.1016/j.jpowsour.2011.04.015

Carbon, MI) and $NaNO_3$ (1 g; Aldrich, >99%) were mixed, then put into concentrated H_2SO_4 (96 ml; Fisher Scientific, 98%) in an ice bath. Under vigorous stirring, $KMnO_4$ (6 g; Fisher Scientific, 99.6%) was gradually added and the temperature of the mixture was kept below 20 °C. After removing the ice bath, the mixture was stirred at 35 °C in a water bath for 18 h. As the reaction progressed, the mixture became pasty with a brownish color. 150 ml H_2O was then slowly added to the pasty mixture. Addition of water into the concentrated H_2SO_4 medium generates large amounts of heat; therefore water should be added slowly and while keeping the mixture in an ice bath to maintain the temperature below 50 °C. After dilution with 240 ml H_2O, 5 ml of 30% H_2O_2 (Fisher Scientific) was added to the mixture, and the color of this diluted solution became a brilliant yellow. After continuously stirring for 2 h, the mixture was filtered and washed with 10% HCl (aq) (250 ml; Fisher Scientific), then DI water and then ethanol (Fisher Scientific, anhydrous) to remove other ions [18]. Finally, the resulting solid was dried under vacuum.

2.2. Prepararion of reduced graphene oxide–SnO_2 composite (RG-O/SnO_2)

The RG-O/SnO_2 composite was prepared by homogeneous precipitation with urea and subsequent reduction with hydrazine under microwave irradiation. In a typical experiment, 1 mmol $SnCl_4{\cdot}6H_2O$ (0.36 g; Fisher Scientific, 98%) and 2 mmol urea (1.20 g; Aldrich, 98%) were separately dissolved in 25 ml water. Then these urea and $SnCl_4$ solutions were slowly and sequentially added to 50 ml of graphite oxide suspension (2 mg ml^{-1}) under stirring, respectively. After exposure to ultrasound from an ultrasonic bath (VWR, B2500A-MT) for 30 min, the mixture was put in a microwave oven (Sensor Microwave Oven, DE68-00307A) and irradiated for 60 s. When cooling to ambient temperature, 0.5 ml N_2H_4 (Aldrich, 64–65%) was added to the mixture while it was being continuously stirred. After that, the mixture was then put into the microwave oven and irradiated for an additional 60 s. The mixture color changed from black-brown to black. Once the reaction was completed, the product was collected by filtration. The as-prepared product was washed several times with DI water to remove the excess hydrazine as well as other ions. In order to obtain good crystallinity, the product was annealed at 500 °C for 3 h in a tube furnace under an atmosphere of nitrogen. For comparison, SnO_2 without RG-O was also synthesized using the same process.

2.3. Characterization

The structure of the obtained RG-O/SnO_2 composite was characterized by X-ray diffraction (XRD) (X'pert, Philips) using CuKα radiation. SEM investigations were performed using an FEI Quanta-600 FEG Environmental SEM. Micro Raman measurements were carried out using a WiTec Alpha 300 system with a 532-nm wavelength incident laser light. Thermal gravimetric analysis (TGA) was done with a Perkin-Elmer TGA 4000 using a heating rate of 5 °C min^{-1} under 20 ml min^{-1} air flow. X-ray photoelectron spectroscopy (XPS) analysis was performed using a Kratos AXIS Ultra DLD XPS equipped with a 180° hemispherical energy analyzer to characterize the particles' surface. Photoemission was stimulated by monochromated Al Kα radiation (1486.6 eV) with an operating power of 150 W. It was operated in the analyzer mode at 80 eV for survey scans and 20 eV for detailed scans of core level lines. Binding energies were referenced to the C 1 s binding energy set at 284.5 eV.

2.4. Electrochemical characterization

Electrochemical experiments were performed using 2032 coin-type cells. The working electrode consisted of 95 wt% active material and 5 wt% polytetrafluoroethylene binder. The electrolyte was a solution of 1 M $LiPF_6$ in EC/DEC (1:1 by volume) (purchased from Novolyte). Pure Li foil (Aldrich) was used as the counter electrode and the separator was Celgard 2300. The cells were discharged and charged galvanostatically for a voltage window from 0.005 to 2.0 V using a Land battery tester (China) at room temperature.

3. Results and discussion

As shown in Scheme 1, graphite oxide prepared by a modified Hummers method [19,20], was sonicated in water to form a suspension of G-O platelets. For the synthesis of the RG-O/SnO_2 composite, $SnCl_4$ was hydrolyzed in the G-O suspension in the presence of urea under microwave irradiation. The molar ratio of $SnCl_4$ to urea was 1:2. This step yielded a uniform $Sn(OH)_4$ or SnO_2 coating on the surface of the G-O platelets. During hydrolysis, urea releases hydroxyl ions slowly and uniformly in the suspension, resulting in the formation of $Sn(OH)_4$, and subsequent decomposition of $Sn(OH)_4$ to SnO_2 as suggested by the following reactions:

$$CO(NH_2)_2 + 3H_2O \rightarrow 2NH_4^+ + CO_2 + 2OH^- \quad (1)$$

$$Sn^{4+} + 4OH^- \rightarrow Sn(OH)_4 \quad (2)$$

$$Sn(OH)_4 \rightarrow SnO_2 + 2H_2O \quad (3)$$

The $Sn(OH)_4$ and SnO_2 particles so produced likely anchor onto the surface of the G-O platelets through oxygen-containing functional groups, such as hydroxyl, epoxyl, and carboxyl.

After the suspension was cooled to room temperature, a trace of hydrazine was added to the suspension under continuous stirring and the suspension again exposed to microwave irradiation. During this process, G-O is converted into RG-O, and the $Sn(OH)_4$ decomposes to SnO_2 nanoparticles as indicated in Eq. (3). The as-prepared composite obtained was characterized by XRD (see Fig. S1). The characteristic peaks of SnO_2 appear but are broad and weak, indicating the SnO_2 particles are amorphous and/or very small in size. In an attempt to improve the crystallinity of SnO_2 particles in the composite, the product was annealed at 500 °C for 3 h in a N_2 atmosphere. XRD of the annealed composite material shows that the diffraction peaks of crystalline SnO_2 nanoparticles are clearly distinguishable, and could be indexed to the tetragonal SnO_2 phase (JCPDS 41-1445). The bonding nature can also be proven by the bonding states of Sn atoms as determined from Sn 3d spectrum. The Sn $3d_{5/2}$ and $3d_{3/2}$ spectrum is composed of single peak, respectively (see Fig. S2). And the Sn peak positions at ~487.03 eV for $3d_{5/2}$, and at ~495.53 eV for $3d_{3/2}$ agree with the presence of SnO_2 [21]. The Raman spectrum has the characteristic peaks of the tetragonal phase of SnO_2 and the D and G peaks of RG-O (see Fig. S3). The composite is 20 wt% RG-O as measured by TGA (see Fig. S4).

The morphology of the as-prepared RG-O/SnO_2 and RG-O/SnO_2 composite was observed by scanning electron microscopy in Fig. 1. Fig. 1a and b shows that the as-prepared RG-O/SnO_2 composite consists of thin, crumpled RG-O platelets closely connected with each other to form a 3D network structure. It is too small for SnO_2 nanoparticles to be seen on the curved RG-O platelets. After annealing at 500 °C, the SnO_2 particle size increases to 100–200 nm in diameter, which can be seen from Fig. 1c and d. Fig. 1c and d also shows that SnO_2 nanoparticles are uniformly distributed on the surface of the RG-O platelets, and can thus act as spacers to prevent the restacking of individual RG-O platelets.

To measure the performance of the RG-O/SnO_2 composite as an anode for Li ion batteries, the composite was mixed with polytetrafluoroethylene (PTFE) in a weight ratio of 95:5 for preparing a working electrode, which is equivalent to a SnO_2:RG-O:PTFE ratio of 76:19:5. Despite increasing the conductivity by adding those into

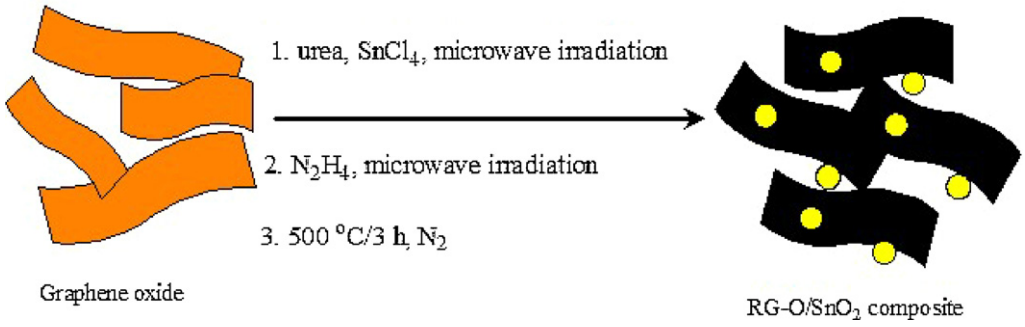

Scheme 1. Scheme for making RG-O/SnO_2 nanoparticle composite.

the electrodes, carbon black or other conductive fillers can also lower the weight specific capacity of the electrode. In our study, carbon black (CB) was not added to the electrode, in contrast to other studies [16,17,22].

Fig. 2a shows the initial two discharge and charge curves of the RG-O/SnO_2 composite at a current density of 50 mA g^{-1} in a voltage range of 2.0–0.005 V *vs.* Li^+/Li. The RG-O/SnO_2 composite delivers 2140 mAh g^{-1} and 1080 mAh g^{-1} capacities for the first discharge and charge, respectively, based on the mass of SnO_2 in the composite (The values are 1712 and 864 mAh g^{-1}, respectively, based on the total mass of the RG-O/SnO_2 composite). It can also be seen that the second discharge and charge capacities are 1105 and 1009 mAh g^{-1}, respectively. According to Fig. 2a, the differential discharge and charge capacity of the initial two cycles *vs* voltage profiles of the RG-O/SnO_2 composite are presented in Fig. 2b. During the first discharge, the reduction peak at 0.95 V corresponds to the formation of a solid electrolyte interface (SEI) layer and Li_2O, and disappears after the first cycle. The reduction peak at 0.24 V corresponds to the formation of Li_xSn alloys [21]:

$$4Li^+ + SnO_2 + 4e^- \rightarrow 2Li_2O + Sn \quad (4)$$

$$xLi^+ + Sn + xe^- \rightleftharpoons Li_xSn \quad (0 \leq x \leq 4.4) \quad (5)$$

After the first discharge, the oxidation peak at 0.50 V and 1.28 V during charging, and the reduction peaks at 1.00 V and 0.24 V during the subsequent discharging, are related to the decomposition and formation of various Li_xSn alloys as described in Eq. (5).

For the complete reduction of $SnO_2 \rightarrow Li_xSn$ ($0 \leq x \leq 4.4$), one would expect a maximum uptake of 8.4Li/SnO_2 (~1494 mAh g^{-1}). For this reaction, 4Li results from the formation of Li_2O (Eq. (4)), and 4.4Li are due to the formation of Li_xSn alloys (Eq. (5)). After the first cycle, it should have 4.4Li theoretical capac-

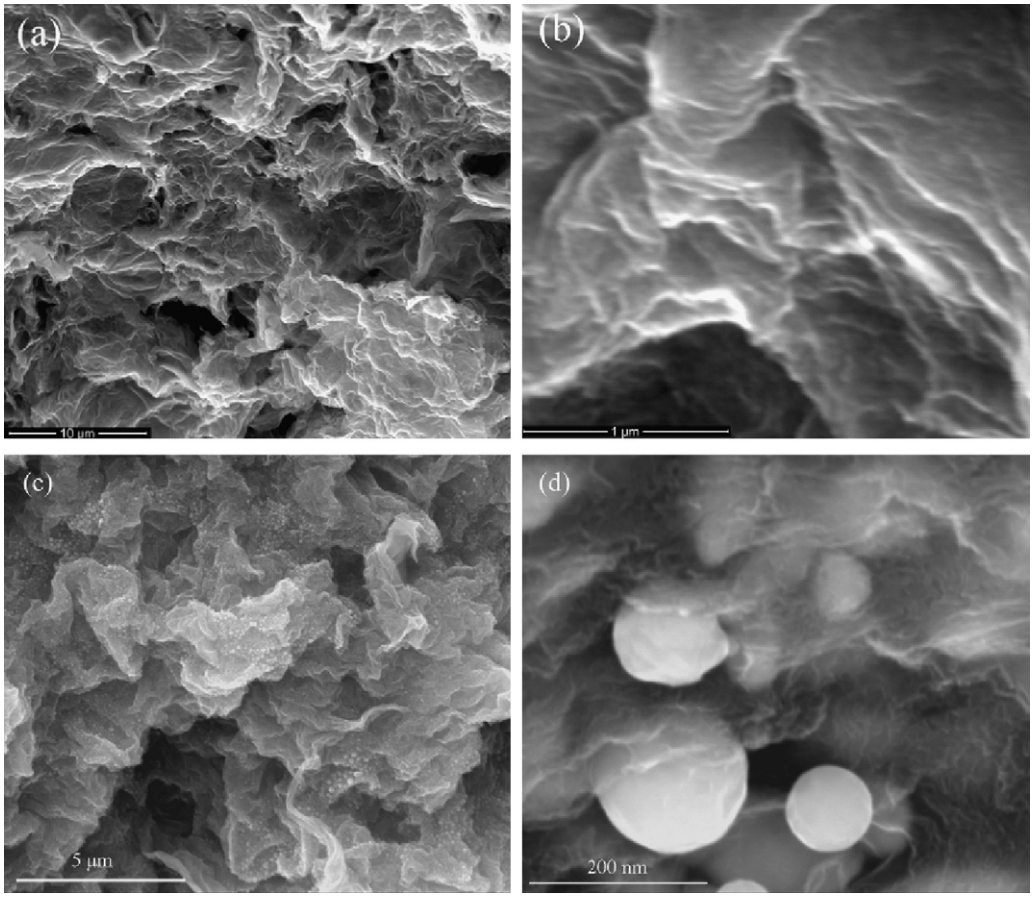

Fig. 1. SEM images of (a and b) unannealed RG-O/SnO_2, and (c and d) RG-O/SnO_2.

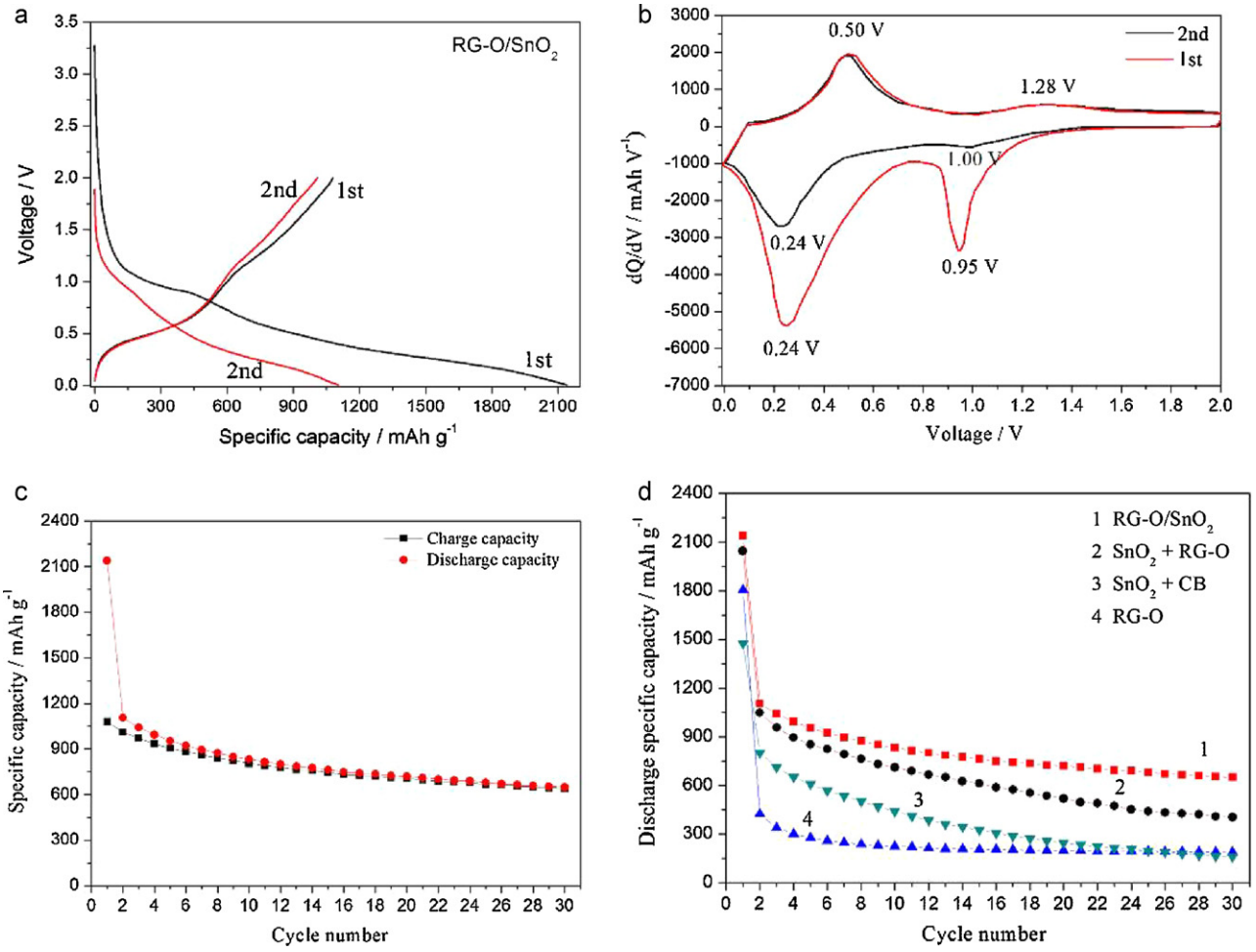

Fig. 2. Electrochemical performance of the RG-O/SnO_2 composite. The specific capacities are based on the mass of SnO_2 in the composite. (a) Discharge/charge profiles of RG-O/SnO_2 for the first and second cycles at the current density of 50 mA g^{-1}. (b) Derivative curves of the first and second cycles for RG-O/SnO_2. (c) Cycling performance of RG-O/SnO_2 composite at a current density of 50 mA g^{-1}. (d) Comparison of cycling performance of RG-O/SnO_2, SnO_2 mixed physically with RG-O, SnO_2 mixed physically with carbon black (CB) in the same weight ratio as RG-O/SnO_2, and RG-O.

ity (~782 mAh g^{-1}). However, the 2140 mAh g^{-1} capacity on the first discharge is higher than 1494 mAh g^{-1}, and 1080 mAh g^{-1} capacity on the first charge is higher than 782 mAh g^{-1}. What gives rise to this 'excess capacity'? The excess capacity appears to originate from electrolyte decomposition in the low-potential region, and thus perhaps the subsequent formation of an organic layer on the surface of the particles [23,24], as well as Li insertion/extraction (or simple decoration on open surfaces) of the RG-O platelets. The Li insertion/extraction/decoration on the surface of RG-O may play a major role in the overall electrochemical process and could be the primary reason for the excess capacity of the RG-O/SnO_2 composite electrode. By comparison, the first cycle of various other types of composites (see Fig. S5) shows that the first charge capacity of 1080 mAh g^{-1} for RG-O/SnO_2 is higher than that of 1020, 430 and 767 mAh g^{-1} for SnO_2 mixed physically with RG-O (indicated as SnO_2 + RG-O), for RG-O itself, and for SnO_2 mixed physically with carbon black (indicated as SnO_2 + CB), respectively. The results indicate that the RG-O/SnO_2 composite has more lithium insertion/extraction sites. This is perhaps because the SnO_2 nanoparticles are anchored on the surface of the RG-O platelets and thus can act as spacers between the RG-O platelets during discharging and charging, leading to higher discharge and charge capacities.

Fig. 2c shows the cycle performance of the RG-O/SnO_2 composite at 50 mA g^{-1} between 2.0 and 0.005 V. The discharge capacities of the electrode in the first, 10th, 20th and 30th cycles are 2140, 834, 720 and 649 mAh g^{-1}, respectively, showing that the RG-O/SnO_2 composite has a much higher capacity than graphite. The coulombic efficiency of the first cycle is 50.5%. After 10 cycles, the coulombic efficiency is greater than 97%, which is higher than 91% of "SnO_2 + RG-O", indicating that the composite has good capacity retention (see Fig. S6).

The high capacity and good cycling stability of the RG-O/SnO_2 composite as an anode material are attributed to the intimate contact between the SnO_2 nanoparticles and RG-O platelets. The uniform mixture and interaction between SnO_2 nanoparticles and RG-O platelets can accommodate the volume change of the nanoparticles during discharging and charging, and prevents the aggregation of the nanoparticles (see Fig. S7) as well as the restacking of RG-O platelets, which likely enhances cycle stability.

A comparison of the discharge cycling performance of RG-O/SnO_2, SnO_2 + RG-O, RG-O, and SnO_2 + CB is shown in Fig. 2d. After 30 cycles, RG-O shows about 44.2% retention (187 mAh g^{-1}) of the second discharge capacity (423 mAh g^{-1}), whereas the SnO_2 + CB composite exhibits about 20.0% retention (160 mAh g^{-1}) of the second discharge capacity (801 mAh g^{-1}). It shows that the specific capacity of SnO_2 + CB fades faster than that of RG-O. On the other hand, RG-O/SnO_2 Exhibits 1105 mAh g^{-1} for the second discharge capacity, higher than 1048 mAh g^{-1} of SnO_2 + RG-O. Furthermore, its cyclic performance is significantly enhanced as

seen from curve 1 in Fig. 2d. After 30 cycles, the discharge capacity was 649 mAh g^{-1}, while the specific capacity of SnO_2 + RG-O was 404 mAh g^{-1}. SnO_2 + RG-O decreased faster than RG-O/SnO_2 during cycling. The comparison of the cyclic performance among RG-O/SnO_2, RG-O, SnO_2 + RG-O and RG-O + CB composites shows that the total specific capacity of the RG-O/SnO_2 composite is higher than the sum of individual SnO_2 and RG-O materials, or that of SnO_2 + RG-O in the same weight ratios, indicating a positive synergistic effect of RG-O platelets and SnO_2 nanoparticles in the composite for enhanced electrochemical performance.

4. Conclusions

In summary, a simple approach is used to fabricate a composite composed of RG-O platelets decorated with SnO_2 nanoparticles for use as a Li-ion battery anode. This RG-O/SnO_2 composite has a capacity of 2140 mAh g^{-1} and 1080 mAh g^{-1} for the first discharge and charge, respectively, at a current density of 50 mA g^{-1}, and good capacity retention with a capacity of 649 mAh g^{-1} after 30 cycles. Our synthesis method can be readily adapted to prepare other composites containing RG-O as a conducting additive that, in addition to supporting metal oxide nanoparticles, can also provide additional Li binding sites to further enhance capacity.

Acknowledgements

This work was supported by the University of Texas at Austin, the U.S. Department of Energy, Office of Basic Energy Sciences, Division of Materials Sciences and Engineering under Award DE-SC001951, the National Science Foundation (DMR-0907324), the China Scholarship Council Fellowship, and the Project-sponsored by SRF for ROCS, SEM.

Appendix A. Supplementary data

Supplementary data associated with this article can be found, in the online version, at doi:10.1016/j.jpowsour.2011.04.015.

References

[1] H. Buqa, D. Goers, M. Holzapfel, M.E. Spahr, P. Novak, J. Electrochem. Soc. 152 (2005) A474–A481.
[2] G. Derrien, J. Hassoun, S. Panero, B. Scrosati, Adv. Mater. 19 (2007) 2336–2340.
[3] J. Hassoun, G. Derrien, S. Panero, B. Scrosati, Adv. Mater. 20 (2008) 3169–3175.
[4] M. Winter, J.O. Besenhard, Electrochim. Acta 45 (1999) 31–50.
[5] J. Fan, T. Wang, C. Yu, B. Tu, Z. Jiang, D. Zhao, Adv. Mater. 16 (2004) 1432–1436.
[6] Y. Wang, J.Y. Lee, H.C. Zeng, Chem. Mater. 17 (2005) 3899–3903.
[7] X.M. Wei, H.C. Zeng, Chem. Mater. 15 (2002) 433–442.
[8] C.-C. Chang, S.-J. Liu, J.-J. Wu, C.-H. Yang, J. Phys. Chem. C 111 (2007) 16423–16427.
[9] Y. Fu, R. Ma, Y. Shu, Z. Cao, X. Ma, Mater. Lett. 63 (2009) 1946–1948.
[10] S. Garaj, W. Hubbard, A. Reina, J. Kong, D. Branton, J.A. Golovchenko, Nature 467 (2010) 190–193.
[11] S. Stankovich, D.A. Dikin, G.H.B. Dommett, K.M. Kohlhaas, E.J. Zimney, E.A. Stach, R.D. Piner, S.T. Nguyen, R.S. Ruoff, Nature 442 (2006) 282–286.
[12] A.K. Geim, Science 324 (2009) 1530–1534.
[13] X.S. Li, W.W. Cai, J.H. An, S. Kim, J. Nah, D.X. Yang, R. Piner, A. Velamakanni, I. Jung, E. Tutuc, S.K. Banerjee, L. Colombo, R.S. Ruoff, Science 324 (2009) 1312–1314.
[14] J.R. Miller, R.A. Outlaw, B.C. Holloway, Science 329 (2010) 1637–1639.
[15] D.H. Wang, D.W. Choi, J. Li, Z.G. Yang, Z.M. Nie, R. Kou, D.H. Hu, C.M. Wang, L.V. Saraf, J.G. Zhang, I.A. Aksay, J. Liu, ACS Nano 3 (2009) 907–914.
[16] H. Wang, L.-F. Cui, Y. Yang, H. Sanchez Casalongue, J.T. Robinson, Y. Liang, Y. Cui, H. Dai, J. Am. Chem. Soc. 132 (2010) 13978–13980.
[17] S.M. Paek, E. Yoo, I. Honma, Nano Lett. 9 (2009) 72–75.
[18] F. Kim, J.Y. Luo, R. Cruz-Silva, L.J. Cote, K. Sohn, J.X. Huang, Adv. Funct. Mater. 20 (2010) 2867–2873.
[19] S. Stankovich, R.D. Piner, S.T. Nguyen, R.S. Ruoff, Carbon 44 (2006) 3342–3347.
[20] W.S. Hummers, R.E. Offeman, J. Am. Chem. Soc. 80 (1958) 1339.
[21] X.J. Zhu, Z.P. Guo, P. Zhang, G.D. Du, R. Zeng, Z.X. Chen, H.K. Liu, ChemPhysChem 10 (2009) 3101–3104.
[22] G.M. Zhou, D.W. Wang, F. Li, L.L. Zhang, N. Li, Z.S. Wu, L. Wen, G.Q. Lu, H.M. Cheng, Chem. Mater. 22 (2010) 5306–5313.
[23] S.R. Mukai, T. Hasegawa, M. Takagi, H. Tamon, Carbon 42 (2004) 837–842.
[24] W.B. Xing, J.R. Dahn, J. Electrochem. Soc. 144 (1997) 1195–1201.